

Seismic cracking evolution for anti-seepage face slabs in concrete faced rockfill dams based on cohesive zone model in explicit SBFEM-FEM frame

Yongqian Qu^{a,b}, Degao Zou^{a,b,*}, Xianjing Kong^{a,b}, Xiang Yu^c, Kai Chen^{a,b}

^a State Key Laboratory of Coastal and Offshore Engineering, Dalian University of Technology, Dalian, 116024, China

^b School of Hydraulic Engineering, Dalian University of Technology, Dalian, 116024, China

^c School of Water Conservancy and Environment, Zhengzhou University, Zhengzhou, 450001, China

ARTICLE INFO

Keywords:

Concrete faced rockfill dam
Slab cracking
Cohesive zone model
Elasto-plastic analysis
Explicit analysis

ABSTRACT

It is critically importance to accurately locate vulnerable areas and quantitatively assess the damage of the face slab in the seismic safety evaluation of concrete faced rockfill dams (CFRDs). In this paper, the cohesive zone model (CZM) is augmented with generalized plastic models of the rockfill and state-dependent elasto-plastic model of the interface to investigate the seismic cracking evolution in the slab of CFRDs. An explicit coupled scaled boundary finite element method-finite element method (Explicit SBFEM-FEM) is developed to enable cross-scale analysis. The method considers the strain softening of rockfill and concrete after being damaged, and avoids negative stiffness and convergence problems that can be found during implicit analysis. A fine, cross-scale model of the CFRD is established based on the quadrature technique. Subsequently, simulations of the construction and impoundment processes are performed to facilitate dynamic analysis. In the first step, different damping ratios for the slab are simulated to optimize accuracy and efficiency. Then, the seismic cracking evolution of the slab is investigated in detail with consideration to the ground motion intensity and steel reinforcement. The results indicate that the computational efficiency can be significantly improved by decreasing the damping ratio of the concrete face slab in the explicit seismic analysis. Penetrating cracks are observed on the slab and the crack reaches maximum width during the earthquake. A residual width is retained after the earthquake. The simulated failure mode of face slab conforms to the characteristics of concrete. The developed method can help precisely locate weak areas of face slab, quantitatively determine the damage severity, and evaluate the ultimate seismic performance of the slab in the CFRDs. In addition, the method can be further employed for concrete cracking analysis involving soil-concrete interaction.

1. Introduction

Hydroelectric power is an important type of renewable energy that is technologically mature and has potential for large scale deployment. Hydroelectricity can help reduce the use of the fossil fuel, optimize the structure of energy consumption, meet society's increasing power requirements, protect the environment, and help with flood control. Therefore, a great number of high dams have been built in many countries [1]. The concrete faced rockfill dam (CFRD) has become a viable dam type for high dam design [2] due to the adaptability to various environments and climates, reliability and economic nature. In actuality, a great number of CFRDs with a height over 100 m are built in areas prone to earthquakes [3], such as the Jinglintai dam (height of 157 m), the Zipingpu dam (height of 156 m), the Longshou II dam (height of 146.5 m), the Jiudianxia dam (height of 133 m), and the

Gongboxia dam (height of 132 m). The above mentioned dams have seismic design intensities greater than VIII. Earthquakes can inflict serious damage to CFRDs and even lead to structural failure, thus putting life, environment, and local properties in danger. Therefore, the seismic safety of the dam is a subject of much attention. The concrete face slab is the chief component of seepage control system in CFRD and can be destroyed during an earthquake, i.e., the dislocation and extruding damage in the slab of Zipingpu CFRD in the Wenchuan earthquake [4,5] and the damage to vertical joint in the Cogoti CFRD in 1943 [6]. The safety and integrity of the face slab is therefore key to ensure the normal operation of the dam. A better understanding of the seismic failure mechanism and quantitative assessment of slabs can aid in preventing catastrophic failures via an improved design of future dams.

Concrete is a quasi-brittle material, and thus when the load is small,

* Corresponding author. State Key Laboratory of Coastal and Offshore Engineering, Dalian University of Technology, Dalian, 116024, China.

E-mail address: zoudegao@dlut.edu.cn (D. Zou).

<https://doi.org/10.1016/j.soildyn.2020.106106>

Received 28 July 2019; Received in revised form 15 January 2020; Accepted 20 February 2020

Available online 3 March 2020

0267-7261/© 2020 Elsevier Ltd. All rights reserved.

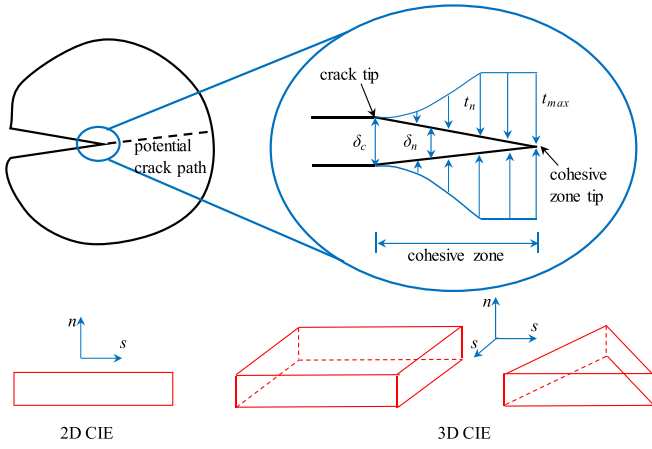


Fig. 1. Cohesive zone model and interface element.

this material behaves with linear elasticity. As the tension increases, the concrete starts to crack and display the characteristics of stiffness degradation and strain softening. In CFRDs, the seismic behavior of the face slab is governed not only by its own properties, but also by the mechanical properties of soil and the interaction between soil and slab [7]. Therefore, compared to a simple concrete structure, the simulation of the damage to a face slab is a more challenging task. Currently, the linear elastic model is widely used to simulate the concrete slab. The model can cause the computed stress to exceed the concrete strength without damage (e.g. cracking) to the concrete, which is unrealistic. Xu et al. [8] and Dakoulas [9] used a plastic damage model [10] to simulate the seismic response of face slabs. The model can reflect the strain softening after the concrete is damaged and qualitatively evaluate the degree of damage. The model treats fractures as a process of damage accumulation and a nonobjective damage factor is applied to describe the damage severity, which cannot be used directly for damage evaluation. Furthermore, the damage factor is scalar, and when damage occurs in one direction, the stiffness and bearing capacity in the other two directions decrease. This problem of the model does not affect two-dimensional analyses but can make it difficult for three-dimensional analyses. Arici [11] applied a fixed cracking model to perform the two-dimensional analysis of the Cokal CFRD, and evaluate the residual crack widths by using other methods. Cen et al. [12] used a damage model to study the influence of the randomness of the materials on the damage of slab; however, the results only estimated the area of damage without quantitatively evaluating the degree of damage.

For the investigation of concrete fracture behavior, the cohesive zone model (CZM) is one of the most commonly used approaches. The concept of CZM was first proposed by Barenblatt [13] and Dugdale [14]. Subsequently, the model was further developed and applied towards concrete cracking simulation by Hillerborg et al. [15]. This model

assumes a small fracture process zone at the crack tip area. In this area, cohesive forces resist the separation of the interface. Stress is treated as a function of displacement during cracking, thus avoiding the singularity issue that has been encountered in many fracture mechanics studies [16]. CZM is based on elasto-plastic mechanics and considers the cracking tip area as a plastic zone. The model can therefore solve problems involving large area yielding at the location of the crack tip. In addition, the model can be simply integrated into numerical computation methods (e.g. finite element method, scale boundary element method, discrete numerical method) [16–18]. Currently, the CZM has been widely used to simulate tension-induced fractural cracks [19–24] and damage in concrete dams [17,24]. However, this model has not yet been applied for analysis of CFRDs.

The thickness of the slab is on the scale of centimeters, but the length of the rockfill area is over several hundred meters, which is orders of magnitudes larger than the slab thickness. While a fine mesh of the slab is necessary in for accurate failure analysis [25,26], a uniform mesh in rockfill area and foundation will generate tens of millions of elements [27]. The large number of elements will result in excessive computational burden. On the other hand, the stress and deformation gradient of the rockfill area is relatively low, and the accuracy requirements can be met without such fine mesh division. Therefore, cross-scale analysis is an effective approach to balance between accuracy and efficiency. Zhou et al. [28] conducted static analysis of a CFRD using a dual-mortar finite element method with mixed tangential contact constraints. Qu et al. [26, 29] proposed an interface element with asymmetric nodes to connect the different mesh size between the slab and the rockfill, and they demonstrated the approach for the dynamic analysis of CFRDs and culverts. Chen et al. [27,30–33] modified the SBFEM to achieve cross-scale static and dynamic analyses of CFRDs.

The primary purpose of this study is to develop a method to describe the evolution of seismic cracking for face slabs in CFRDs. The CZM of concrete is programmed into the analysis platform GEODYNA using C++ and is combined with generalized plastic models of the rockfill and the interface to investigate the seismic cracking evaluation for the slab in CFRDs. An explicit SBFEM-FEM approach is developed to enable cross-scale analysis. The method considers the strain softening of rockfill and concrete after being damaged and avoids negative stiffness and convergence problems that can be found during implicit analysis. The accuracy of the method is validated by a dynamic failure test of a concrete beam. A fine, cross-scale model of the CFRD is established based on the quadrature technique. Subsequently, simulations of the construction and impoundment processes are performed to facilitate dynamic analysis.

In the first step, different damping ratios for the slab are simulated to optimize accuracy and efficiency. Then, the seismic cracking evolution of the slab is investigated in detail with consideration to the ground motion intensity and steel reinforcement. The method developed in this paper can evaluate the potential severity of cracking, precisely locate weak areas of face slabs, and quantitatively evaluate the damage

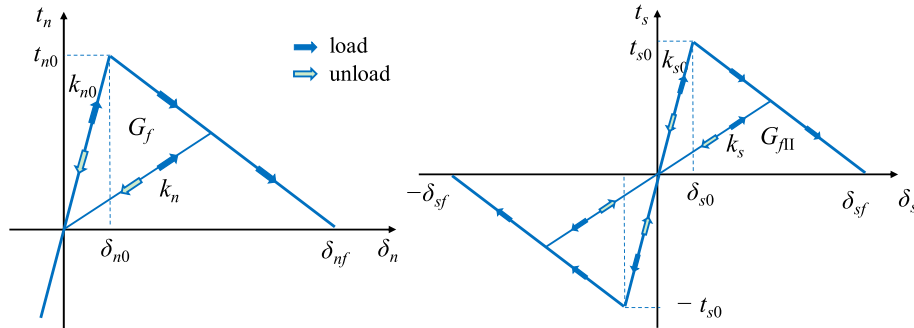


Fig. 2. Relationship between traction and displacement.

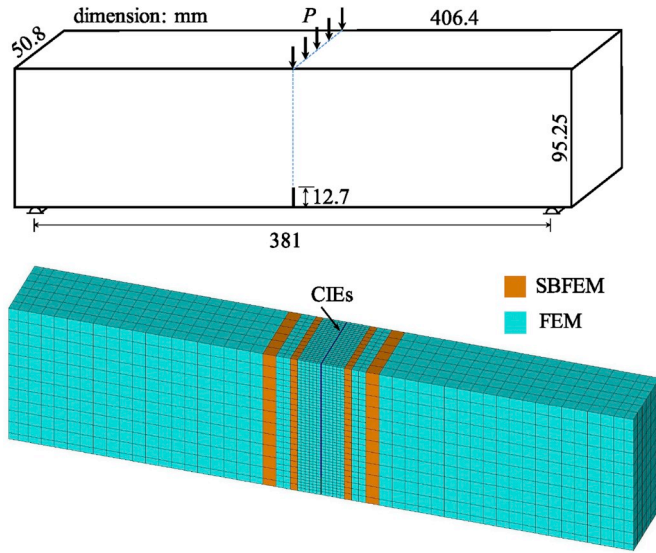


Fig. 3. Geometry and mesh of concrete beam.

severity. The results also provide a foundation for risk assessment (e.g. seepage induced damage, dam collapse) of dams after earthquake. The method can be straightforwardly extended towards three-dimensional analysis and be utilized for other types of anti-seepage concrete structures (e.g. connection plate, anti-seepage wall), as well as concrete cracking analysis involving soil-concrete interaction.

2. Material model and solution method

2.1. Linear cohesive zone model

The CZM is built upon the foundation of elasto-plastic fracture mechanics. This model assumes a small fracture process zone at the crack tip area and employs the relationship between the opening displacement and the surface traction to simulate the mechanical behavior of the interface after cracking. The CZM is shown in Fig. 1, where t is the surface traction and δ is the opening displacement. When the cracking process is simulated, the cohesive interface elements (CIEs) are set along the potential cracking path and are connected to the solid elements. At the early stage of loading, the CIE exhibits linear elastic behavior. As the loading increases, CIE reaches the cracking criteria upon which stiffness and bearing capacity decreases. When the stiffness drops to 0, the elements become invalid and a new crack appears.

In the elastic stage, the stress-displacement relationship is described by:

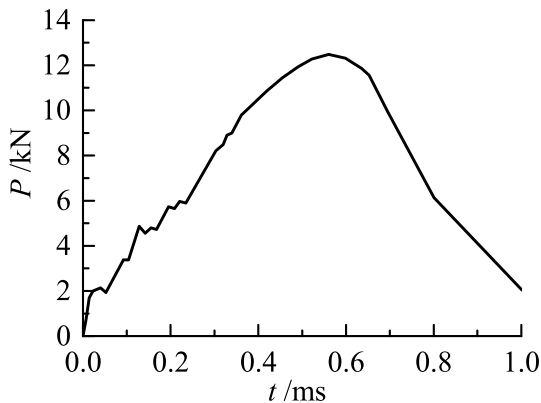


Fig. 4. Measured load history.

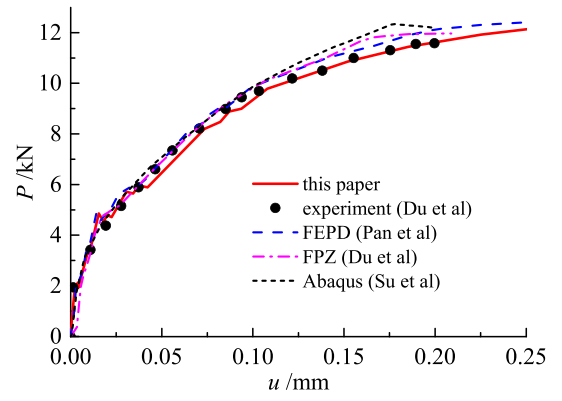


Fig. 5. The relationship between load and the vertical displacement at the loading point.

$$\mathbf{t} = \begin{Bmatrix} t_n \\ t_s \end{Bmatrix} = \begin{bmatrix} k_{n0} & k_{ns0} \\ k_{sn0} & k_{s0} \end{bmatrix} \begin{Bmatrix} \delta_n \\ \delta_s \end{Bmatrix} = \mathbf{K} \boldsymbol{\delta} \quad (1)$$

where, \mathbf{t} is the stress vector, t_n and t_s are the normal and tangential stresses of the cracking, k_{n0} and k_{s0} are the initial normal and tangential modulus, δ_n and δ_s are the normal and tangential displacements, $\boldsymbol{\delta}$ is the displacement vector, and \mathbf{K} is the element stiffness matrix. In a majority of situations, the interaction between the normal and tangential direction is not considered. Thus, k_{ns} and k_{sn} are equal to 0.

When element is damaged, its stiffness degrades. The damage variable d is defined to describe the degree of stiffness degradation, and can be expressed by using the effective displacement δ_m as follows,

$$\delta_m = \sqrt{\langle \delta_n \rangle^2 + \delta_s^2} \quad (2)$$

$$\langle \delta_n \rangle = (\delta_n + |\delta_n|) / 2 \quad (3)$$

$$d = \frac{\delta_f(\delta_{\max} - \delta_0)}{\delta_{\max}(\delta_f - \delta_0)} \quad (4)$$

where δ_0 is the initial cracking displacement, δ_{\max} is the maximum effective displacement in the loading history, and δ_f is the displacement at the failure stage. Therefore, the stress-displacement relationship in the model can be derived as

$$\mathbf{t} = \begin{Bmatrix} t_n \\ t_s \end{Bmatrix} = (1-d)\mathbf{K} \begin{Bmatrix} \delta_n \\ \delta_s \end{Bmatrix} + d\mathbf{K} \begin{Bmatrix} -\delta_n \\ 0 \end{Bmatrix} \quad (5)$$

The fracture energy is the area within the curve shown in Fig. 2 and can be expressed as

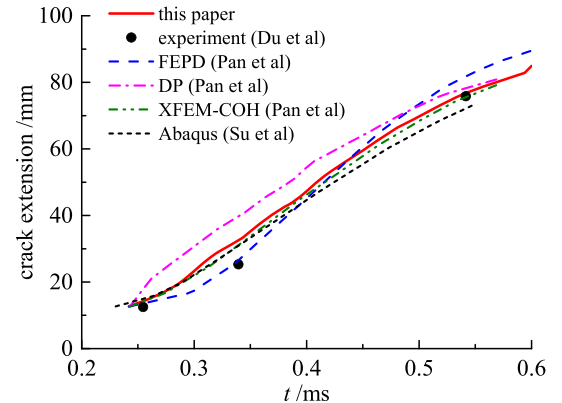


Fig. 6. Crack extension history.

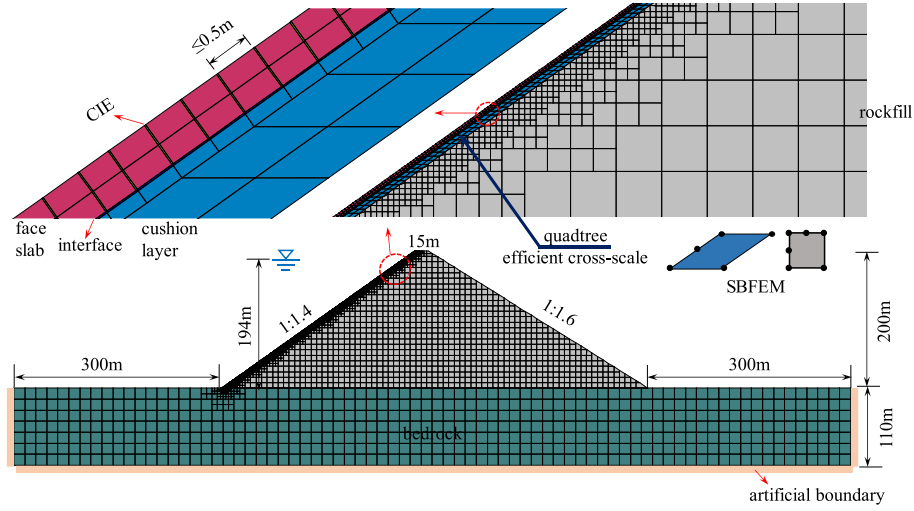


Fig. 7. The mesh and boundary condition for the CFRD model.

Table 1
Parameters used for the rockfill model.

G_0	K_0	M_g	M_f	α_f	α_g	H_0	H_{U0}	m_s
1663	2199	1.6	1.58	0.23	0.2	3000	2800	0.35
m_v	m_l	m_u	r_d	γ_{DM}	γ_u	β_0	β_1	
0.35	0.42	0.3	200	50	9	40	0.012	

Note: All the parameters are dimensionless.

$$G = \int_0^{\delta_f} t(\delta) d\delta = \frac{1}{2} t_0 \delta_f \quad (6)$$

where t_0 is the adhesive strength. The cracking criteria is defined based on the squared criterion of the stress:

$$\left(\frac{t_n}{t_{n0}}\right)^2 + \left(\frac{t_{s1}}{t_{s0}}\right)^2 + \left(\frac{t_{s2}}{t_{s0}}\right)^2 = 1 \quad (7)$$

2.2. Explicit analysis

The most commonly used explicit method in mechanics and physics is the central difference method, which can be expressed as,

$$\Delta t^n = t^n - t^{n-1}, \Delta t^{n+1/2} = (\Delta t^n + \Delta t^{n+1}) / 2 \quad (8)$$

$$\mathbf{v}^{n+1/2} = \mathbf{v}^{n-1/2} + \Delta t^n \mathbf{a}^n \quad (9)$$

$$\mathbf{u}^{n+1} = \mathbf{u}^n + \Delta t^{n+1/2} \mathbf{v}^{n+1/2} \quad (10)$$

where \mathbf{u} , \mathbf{v} , and \mathbf{a} are the displacement, velocity, and acceleration vectors. The superscripts n , $n-1$ and $n+1/2$ refer to the step and half-steps. The acceleration can be further expressed as,

$$\mathbf{a}^n = \mathbf{M}^{-1} (\mathbf{F}^n - \mathbf{I}^n) \quad (11)$$

where \mathbf{M} is the concentrated mass matrix, \mathbf{F} is the external force vector, and \mathbf{I} is the internal force vector.

Table 2
Parameters used for the cushion model.

G_0	K_0	M_g	M_f	α_f	α_g	H_0	H_{U0}	m_s
1265	2021	1.54	1.4	0.25	0.32	2800	2500	0.55
m_v	m_l	m_u	r_d	γ_{DM}	γ_u	β_0	β_1	
0.55	0.4	0.2	150	50	5	35	0.015	

Note: All the parameters are dimensionless.

Table 3
Interface material parameters.

D_{s0}/kPa	D_{n0}/kPa	M_c	e_r	λ	$a/\text{kPa}^{0.5}$	b	c
1000	1500	0.88	0.4	0.091	224	0.06	3.0
a	r_d	k_m	M_f	k	H_0/kPa	f_h	t/m
0.65	0.2	0.6	0.65	0.5	8500	2	0.1

The explicit integration method is conditionally stable. Thus, the time step Δt for the undamped system is defined as,

$$\Delta t \leq \Delta t_{crit} = \frac{2}{\omega_{max}} \leq \min_{e,i} \frac{2}{\omega_i} = \min_e \frac{l_e}{c_e} \quad (12)$$

$$c_e = \sqrt{E_e / \rho_e} \quad (13)$$

where ω_{max} is the maximum frequency of system, l_e is the characteristic length of element e , c_e is the wave velocity of the element e , E_e is the Young's Modulus of the element e , and ρ_e is the density of the element e . For the damped system, the critical step can be expressed as

$$\Delta t \leq \Delta t_{crit} = \min_i \frac{2}{\omega_i} \left(\sqrt{\xi_i^2 + 1} - \xi_i \right) \quad (14)$$

where ω_i is the i th frequency, ξ_i is the damping ratio of the system at the i th frequency.

2.3. Scaled boundary finite element method

The SBFEM is a semi-analytical method that was first proposed by Song and Wolf [34,35], and inherits the advantages of the boundary element method (BEM). This method is inherently appropriate for modelling polygons and polyhedrons with an arbitrary number of nodes and faces. With such an important advantage, the SBFEM can handle more complex geometries than other methods.

A considerable amount of effort has been devoted to extending the applications of SBFEM in elastic problems over the past few years [36–41]. An obstacle towards broad application is that material nonlinearity must be considered to obtain a reasonable solution in many

Table 4
Cohesive zone model parameters.

k_n/GPa	k_s/GPa	C/MPa	$G/\text{N/m}$
31	13.25	3.48	325

Table 5
Parameters used for the face slab and bedrock.

Component	E/GPa	$\rho/\text{kg}\cdot\text{m}^{-3}$	ν
Face slab	31	2500	0.17
Rockfill foundation	10	2400	0.25

engineering structure analyses, particularly for the simulation of geotechnical engineering structures, where nonlinearity is ubiquitous. To circumvent this restriction, an internal integration technique was presented by Chen et al. [30,33] to replace the original boundary integral scheme. In doing so, the researchers provided an alternative method to perform nonlinear analysis using the SBFEM. The method was validated by demonstrating its use on predicting the evolution of damage for several specific examples. In this paper, the SBFEM is modified to explicit frame, and the explicit SBFEM-FEM cross-scale analytical method for CFRDs is established.

2.4. Constitutive models for rockfill and interface

The Pastor-Zienkiewicz model presented by Pastor and Zienkiewicz [42,43] is applicable to the static and seismic response analyses with the uniform parameters and can directly compute earthquake-induced permanent deformations. The researchers modified the volume modulus, the shear modulus, the load modulus, and the unload modulus of this model [44]. The modified model can better describe the stress correlation and cyclic hysteresis, and has been successfully used for the static and dynamic analyses of CFRDs [44–46].

Based on the framework of the generalized plasticity model and the two-dimensional interface model [47,48], Liu et al. [49] developed a three-dimensional state-dependent elasto-plastic model. The model can accurately reflect the deformation characteristics of the interface under monotonous and cyclic loading in three dimensions, including shear contraction, shear dilation, hardening, softening and particle breakage.

3. Numerical example

The dynamic fracture test of concrete beam conducted by Du et al. [50] is simulated to verify the explicit SBFEM-FEM and CZM. The specimen geometry and cross-scale model is shown in Fig. 3. A 12.7 mm long gap is made at the bottom of the beam. Due to the symmetry of structure, constraint conditions and the load, the crack will propagate in the middle of the beam. Therefore, the CIEs are embedded along the potential crack path in the example [19]. The impact load measured in the test as shown in Fig. 4 is applied to the center of the beam. The material properties [17] are as follows: density, $\rho = 2500 \text{ kg/m}^3$; Young's Modulus, $E = 34.48 \text{ GPa}$; Poisson's ratio, $\nu = 0.2$; tensile strength, $f_t = 5.24 \text{ MPa}$, and the fracture energy, $G = 200 \text{ N/m}$.

As shown in Fig. 5, the computed relationship between the load and the load-line displacement of this paper are compared to the experimental results reported in literature. The numerical and experimental results of the crack extension are shown in Fig. 6. The simulated results extracted from literature using fracture process zone (FPZ) model (Du et al. [50]), DP model, plastic damage model, XFEM method (Pan et al.

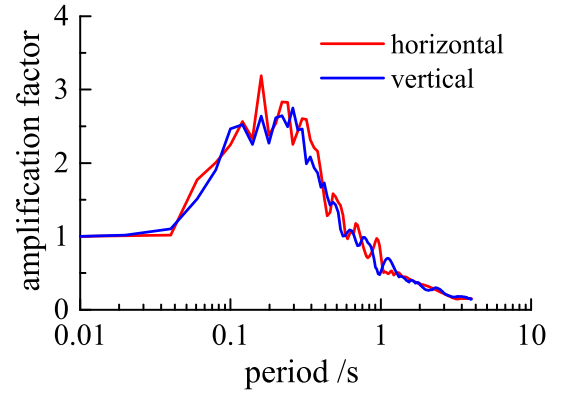


Fig. 9. Response spectrum of the seismic wave.

[17]), and the cohesive crack model in Abaqus (Su et al. [19]) are also plotted in Figs. 5 and 6. The figures show that the computed results of this paper show good agreement with the experimental and numerical results from literature. This example demonstrates that the CZM for concrete is successfully incorporated into the developed procedure, which will guarantee the rationality of the results of the CFRD dynamic analysis.

4. Modelling of the concrete faced rockfill dam

4.1. Finite element model

A two-dimensional model of a CFRD is used for the static and dynamic analysis, as shown in Fig. 7. The upstream and downstream slopes are 1:1.4 and 1:1.6, respectively. The width of the dam crest is 15 m. The depth and width of the foundation are 110 m and 1215 m, respectively. The distance of the lateral boundaries is reasonable and can assure the required precision for dynamic analysis when combined with the non-uniform seismic motion input method [26]. The face slab is 0.3 m thick at the top of the dam, and the thickness at each location on the dam is determined by $d = 0.3 + 0.0035h$, where d is the thickness of the face

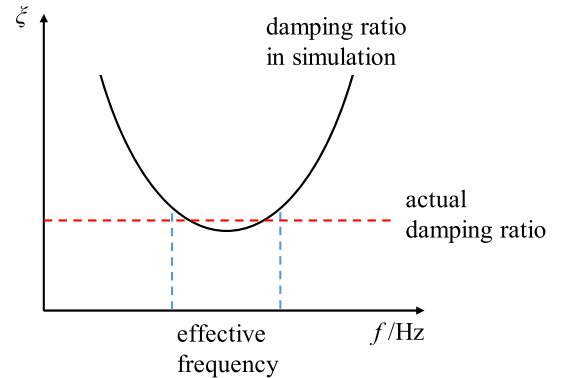
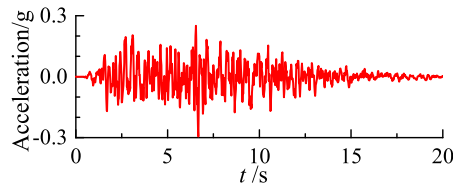
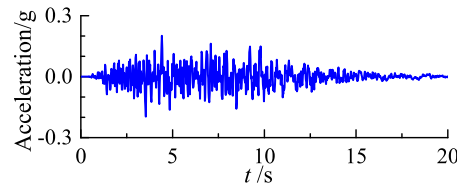


Fig. 10. Relationship between damping ratio and frequency.



(a) horizontal direction



(b) vertical direction

Fig. 8. Input ground motion history.

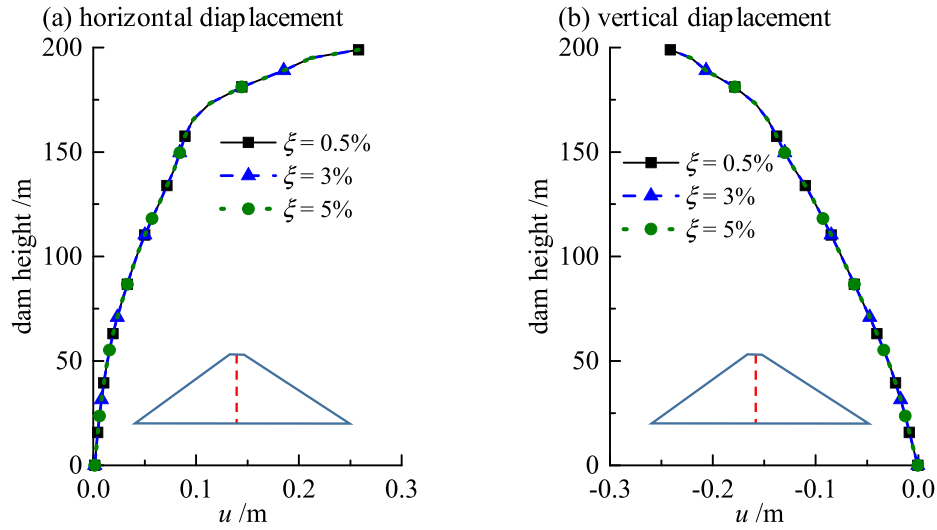


Fig. 11. Influence of face slab damping ratio on the residual displacement along the dam height after the earthquake.

slab and h is the distance between the cross section and the top of the dam. The construction process is divided into 26 steps and the impoundment process is divided into 30 steps. The reservoir is full and the depth of water is 194 m. In order to ensure the accuracy of the simulation, the slab is finely discretized using 4-node isoparametric elements. The mesh of the face slab is divided into 2 layers along the direction of the thickness, and the mesh size of the slab is less than 0.5 m in the direction of the slope. CIEs are set along the slope. Considering the small time step of the explicit analysis, the computational burden is excessive especially for elasto-plastic analysis. To improve the computation efficiency, the SBFEM [51,52] and the quadtree method [53] are

used to build a cross-scale model. The dam body and most of the rock foundation are meshed with 4-node isoparametric elements. A small portion the body is meshed through SBFEM. In order to simulate soil-structure interaction, interface elements are set between the face slab and the cushion. In the dynamic analysis, the added mass method is adopted to consider the hydrodynamic pressure on the face slab [54].

4.2. Material parameters

The parameters of the rockfill and cushion based on large-scale triaxial tests of a CFRD built in China are summarized in Tables 1 and

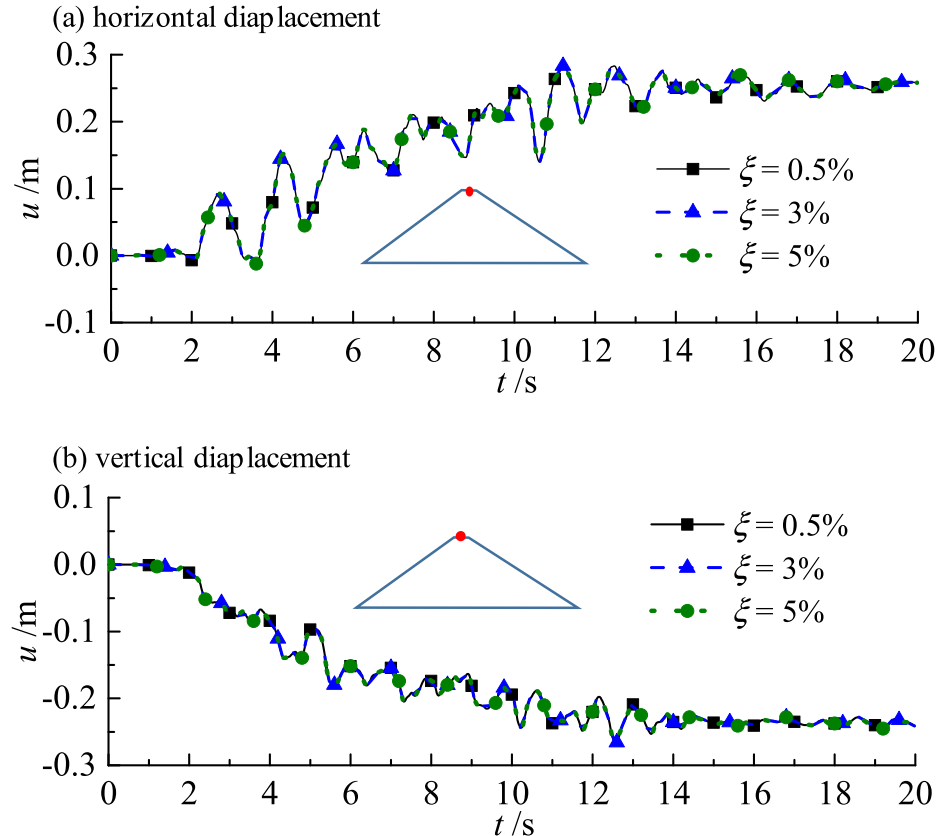


Fig. 12. Influence of face slab damping ratio on the displacement of dam crest during earthquake.

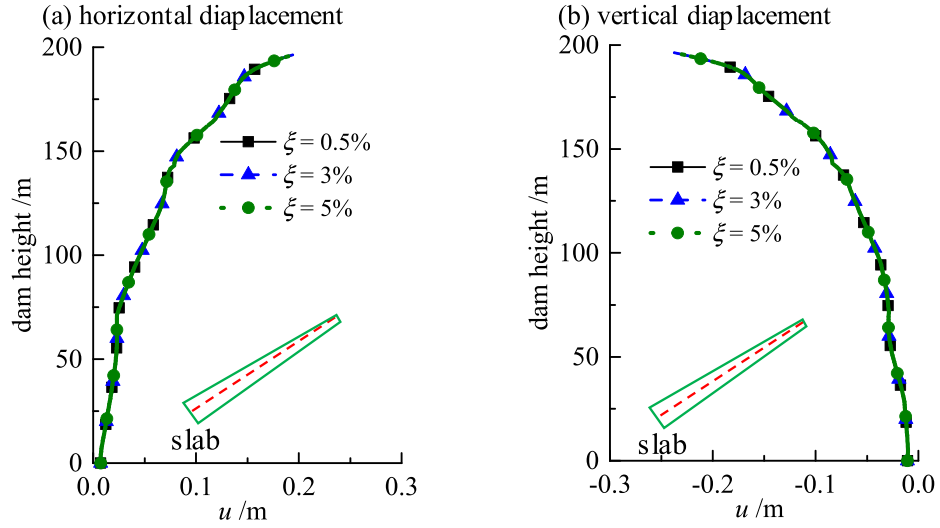


Fig. 13. The maximum dynamic displacements of slab during the earthquake.

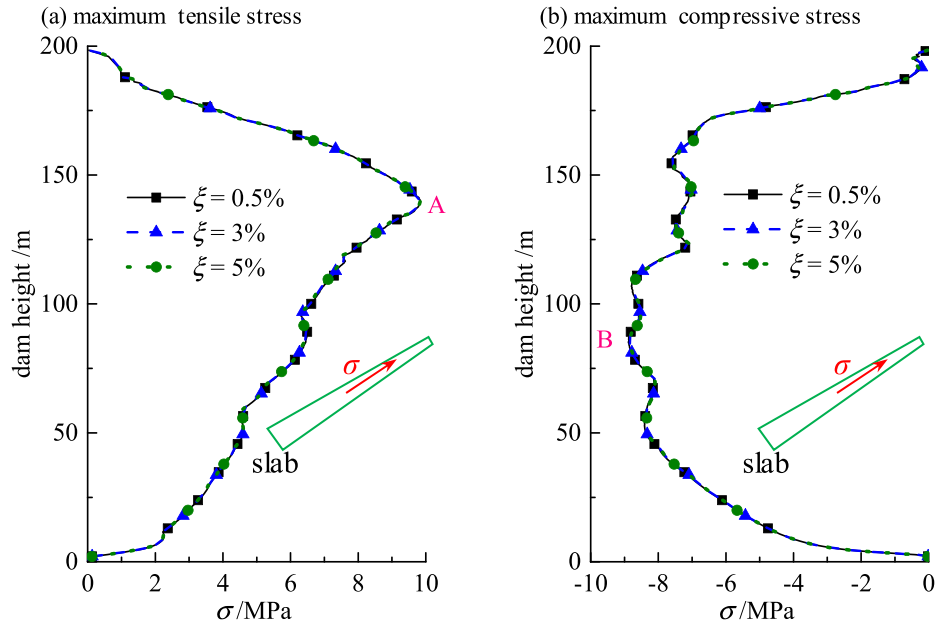


Fig. 14. Influence of face slab damping ratio on the peak dynamic stresses along the slope during the earthquake.

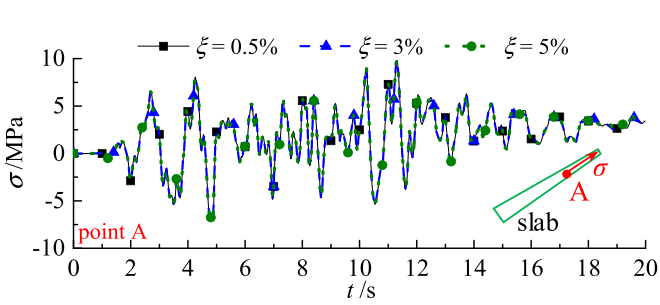


Fig. 15. Time history of dynamic stresses at point A for different face slab damping ratios.

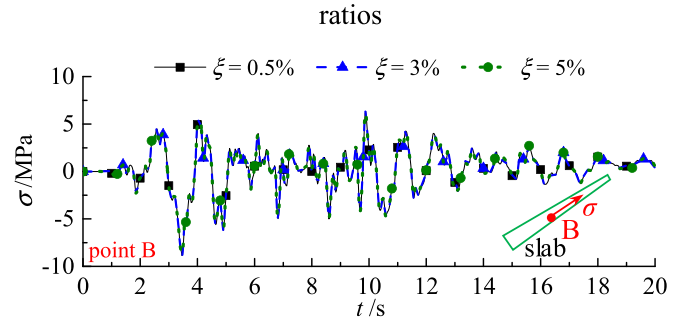


Fig. 16. Time history of dynamic stresses at point B for different face slab damping ratios.

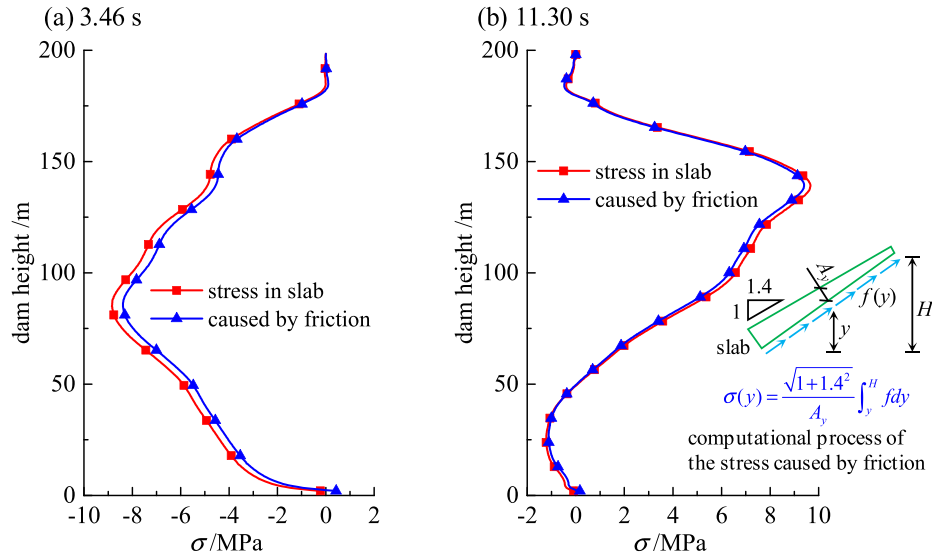


Fig. 17. Actual stresses and the portion induced by friction along the slope.

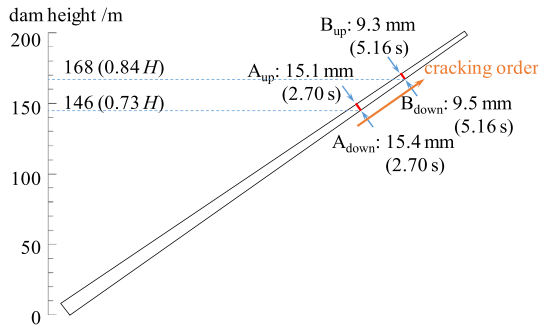


Fig. 18. Crack location, maximum crack width, and initial cracking moment of the concrete face slab during earthquake.

2, respectively. The material parameters [55] of the interface between the face slab and the cushion layer are listed in Table 3. The parameters of CZM are listed in Table 4. The tensile strength and the fracture energy are 3.48 MPa and 325 N/m [8], respectively. A linear elastic model is used for the overlaying bedrock and face slab, and the parameters are listed in Table 5.

4.3. Seismic input

The input ground motion is a simulated earthquake wave based on the response spectrum obtained from the earthquake risk analysis of a CFRD built in China. The peak ground acceleration (PGA) in the

upstream–downstream (horizontal direction) is 0.3 g, and the vertical PGA is 2/3 of the horizontal PGA in the stream direction. The acceleration time history and response spectrum of the seismic wave are shown in Figs. 8 and 9. The non-uniform seismic motion input method [56,57] is applied to simulate the interaction between the dam and the foundation.

4.4. Influence of slab damping ratio

As can be seen from Eq. (14), the time step in the central difference method is inversely proportional to the structural frequency and the corresponding damping ratio. The Rayleigh damping theory [58] is commonly utilized in the dynamic analysis of the CFRD, as shown in the following:

$$\mathbf{C} = \alpha \mathbf{M} + \beta \mathbf{K} \quad (15)$$

$$\xi = \frac{1}{2} \left(\frac{\alpha}{\omega} + \beta \omega \right) \quad (16)$$

where \mathbf{C} is the damping matrix, \mathbf{M} is the mass matrix, \mathbf{K} is the stiffness matrix, ξ is the damping ratio, ω is the circular frequency, and α and β are respectively the damping coefficients of the mass and stiffness matrices. The material damping ratio is not related to the frequency. Therefore, the damping coefficients should be set to ensure that the damping ratio for main frequencies is close to the material property, as shown in Fig. 10 [8,59]. For an example, Hudson and Iriess [60] determined the damping coefficients based on the dominant structural and seismic frequencies.

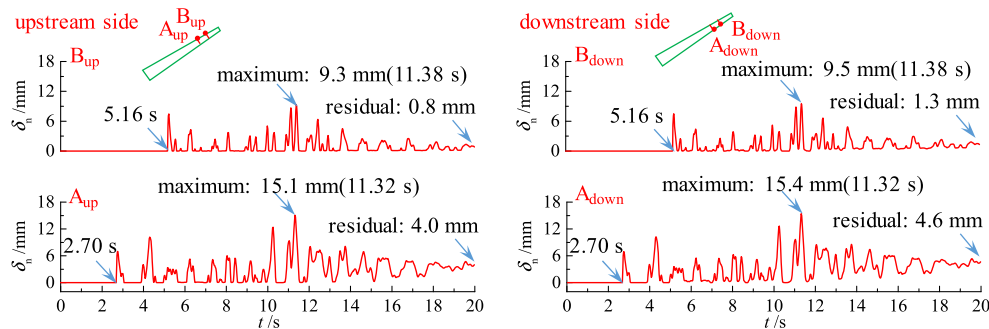


Fig. 19. Crack evolution during the earthquake.

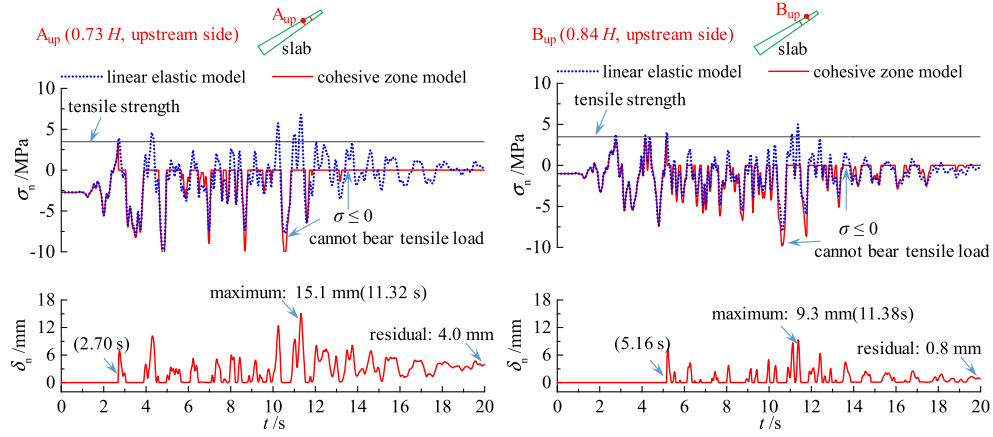


Fig. 20. Crack width and stresses along the slope of the upstream side of face slab during the earthquake.

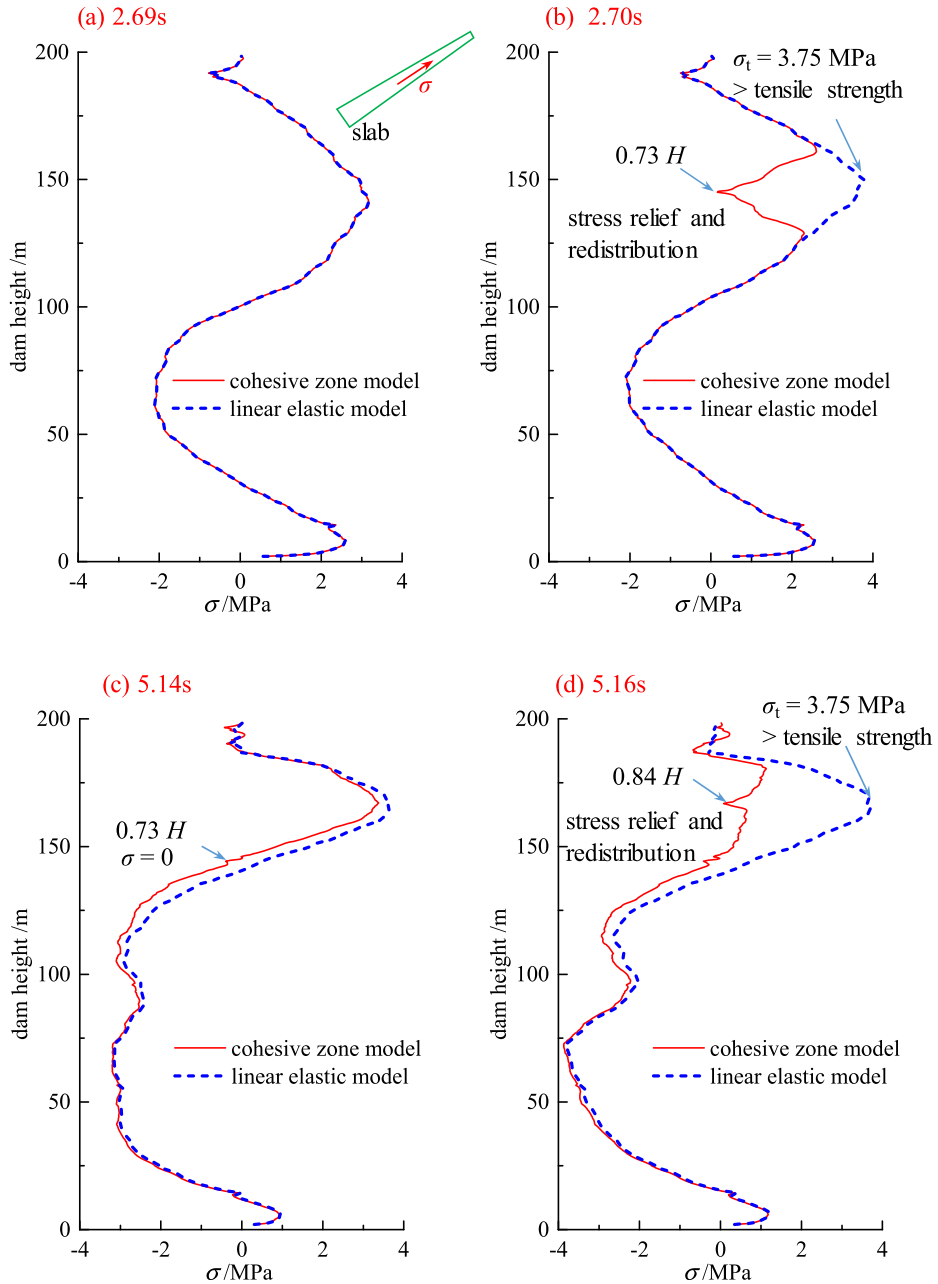


Fig. 21. Stresses along the slope of the face slab at select time points during the earthquake.

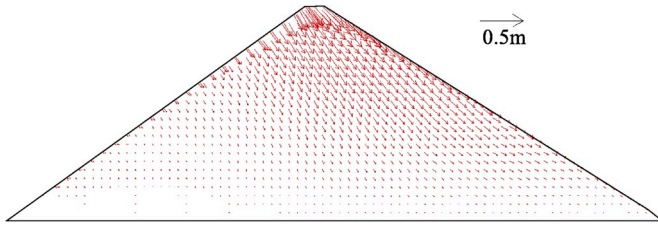


Fig. 22. Vector plot of the dam body deformation after the earthquake.

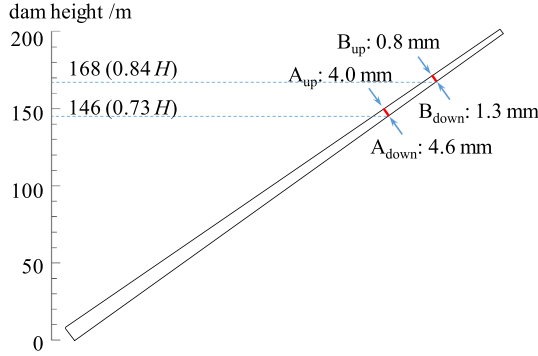


Fig. 23. Distribution of residual crack on face slab after earthquake.

$$\alpha = 2\xi \frac{\omega_1 \omega_2}{\omega_1 + \omega_2} \quad (17)$$

$$\beta = 2\xi \frac{1}{\omega_1 + \omega_2} \quad (18)$$

$$\omega_2 = n\omega_1 \quad (19)$$

where ω_1 is the dominant frequency of the structure, n is an odd value which is greater than ω_e/ω_1 , and ω_e is the dominant frequency of the seismic wave. According to Eq. (16), during the simulation, the damping ratio at high frequencies is excessive, which will decrease the temporary time step and thus greatly reduce the computational efficiency.

In the CFRD, the Young's modulus of the face slab and the bedrock is much larger than that of the rockfill. Furthermore, the mesh size of the face slab is much smaller than that of the bedrock. Therefore, the face slab is a key factor in determining temporary time step of simulation. In addition, the dynamic response of the face slab is not determined by itself, but is rather influenced by the response of the soil and interface between slab and cushion. Therefore, this paper firstly studies the influence of face slab damping ratio on the dynamic response of CFRD without considering the failure of slab.

The residual deformation along the height of the dam after the earthquake is shown in Fig. 11 for different damping ratios of the slab (5%, 3% and 0.5%). The displacement history at the top of dam is shown in Fig. 12. Since the mass and stiffness of the face slab accounts for a very small portion of the entire dam, the change of the damping ratio of the face slab has little effect on the dynamic response of the dam.

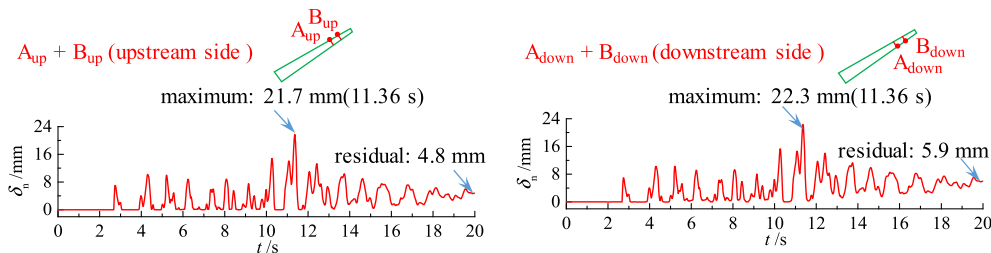


Fig. 24. Evolution of the total crack widths during the earthquake.

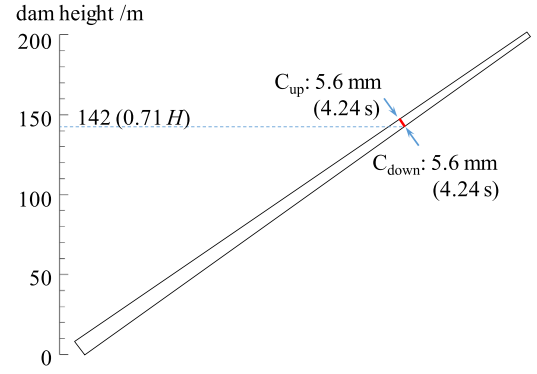


Fig. 25. Crack location, maximum crack width, and initial cracking moment for the reinforced concrete face slab during the earthquake.

The maximum dynamic displacements (induced by earthquake) of each node on slab during earthquake are plotted in Fig. 13. Fig. 14 shows the peak dynamic stress along the slope of the slab during the earthquake for different damping ratios of the slab. In other words, the figure shows the maximum stress of each element during earthquake. Two observation points A and B are set at the maximum tensile and compressive stress locations, respectively. Figs. 15 and 16 show the time history of the dynamic stress along the slope at points A and B. Both the dynamic displacement and stress of slab are almost the same for the different damping ratios of the slab.

The compressive and tensile stresses are maximum at 3.46s and 11.30s, respectively. Fig. 17 shows the actual dynamic stress along the slope of slab and the portion of the stress caused by friction from the soil at the two moments. The computation of the friction-induced dynamic stress along the slope of the slab is shown in Fig. 17(b), where f is the shear force in interface element, A is the area, H is the dam height, and σ is the stress caused by friction. It can be seen from the figure that the dynamic stress along the slope of face slab is mainly generated from the friction. The water in the reservoir acts as a constraint for the slab; therefore, the inertia force of slab is limited during earthquake especially when the reservoir is full. Therefore, the damping ratio of the concrete face slab has limited influence on the stress of the face slab. Fortunately, a reduction of the damping ratio of slab from 5% to 0.5% can significantly improve the time step from 1.5×10^{-7} s to 1.5×10^{-6} s, which is a tenfold improvement in computational efficiency. The results demonstrate that it is feasible to decrease the damping ratio of the face slab to increase the time step and improve the computation efficiency in the explicit dynamic analysis of the CFRD.

5. Dynamic response of CFRD

5.1. Crack evolution analysis

The crack location, maximum crack width and initial cracking moment of the face slab during the seismic response are shown in Fig. 18. The evolution of all the cracks during the earthquake are illustrated in Fig. 19. The cracks are located at 0.73H and 0.84H of the face

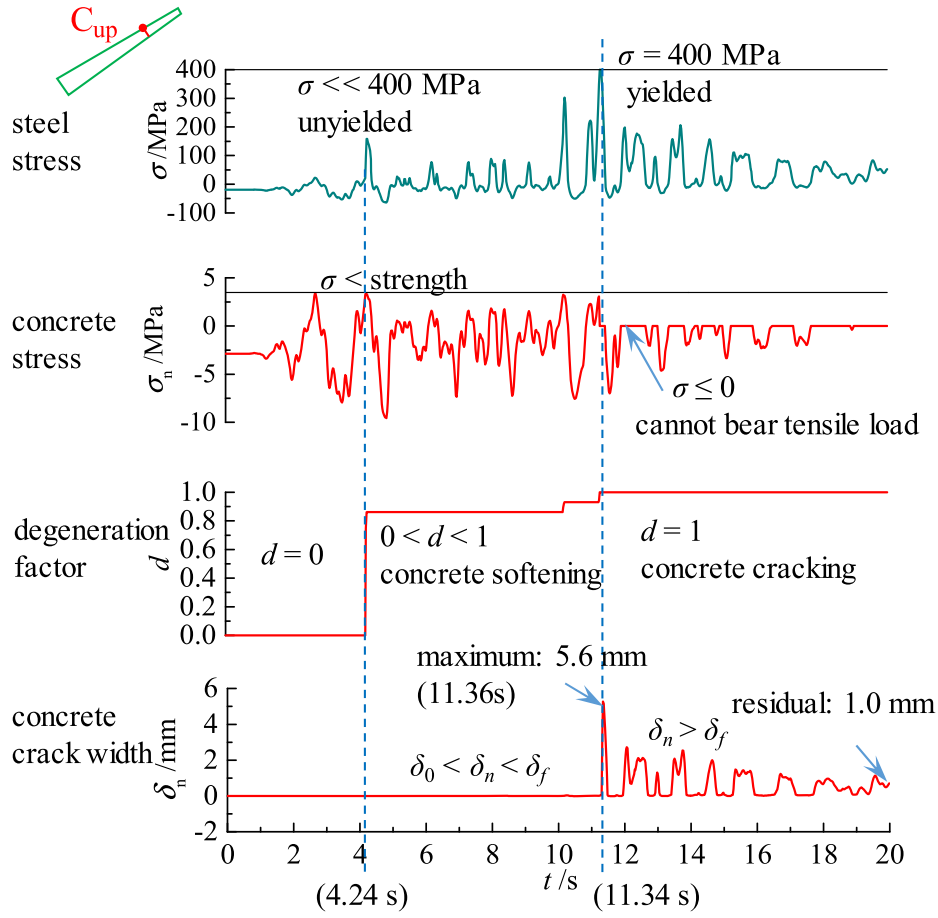


Fig. 26. Time histories of the axial stress of steel, concrete stress along the slope, degeneration factor, and crack width during the earthquake.

slab, where H is the height of the dam. The maximum crack widths corresponding to these two locations are 15.4 mm and 9.5 mm, respectively. The crack propagates through the thickness of the face slab. Thus the slab is fully cracked both in Point A and B. The initial cracking moment at both sides of the face slab are the same. Zhang et al. [61] used a linear elastic model to analyze this problem and found that the extent of tensile overstressed area is $0.5\text{--}0.9H$. Xu et al. [8] obtained similar results based on plastic damage model. The damage location estimated in this research lies within the area predicted by literature, which corroborates each other. Concrete is a quasi-brittle material and the tensile failure mode is localized and narrow-band. The results in this paper provides an accurate damage location and agrees with the damage characteristics of concrete.

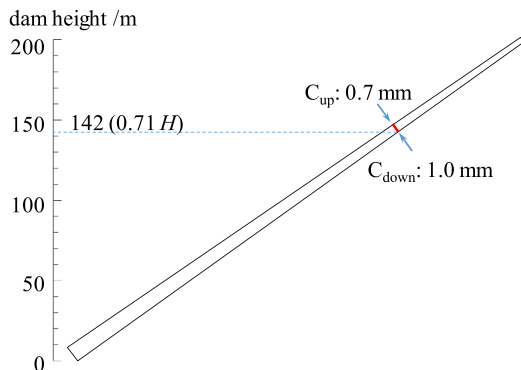


Fig. 27. Crack distribution of the reinforced concrete face slab after the earthquake.

In order to demonstrate the proposed method, numerical results without considering failure of slab (linear elastic model) were also computed and compared with those of the CZM. Fig. 20 shows the time history of the crack width and stress (including the static response) along the slope at $0.73H$ and $0.84H$ of the face slab at the upstream side. The crack at $0.73H$ occurs at 2.70s. The stresses along the slope of the damaged element before and after cracking are provided in Fig. 21(a) and (b). Before cracking, the CIEs remain in the elastic stage, and the behavior for the two investigated models are identical. After cracking, the stress computed from the linear elastic model exceeds the tensile strength and the concrete cracks at the CZM along with a rearrangement of the stress distribution. At 5.16s, the face slab at $0.84H$ starts to crack. The stresses before and after cracking are shown in Fig. 21(c) and (d). Before cracking at $0.84H$, since the crack at $0.73H$ has already occurred, the tension obtained from the CZM is smaller than the one from the linear elastic model. After cracking, the stress computed from the linear elastic model exceeds the tensile strength again and cracking occurs at the CZM along with a relief of the tensile stress. As the of ground motion intensity and the accumulation of residual deformation of dam increases, the crack widths at $0.73H$ and $0.84H$ reach maximum values at 11.36s and 11.40s, respectively. In the later period of the earthquake when the ground motion intensity is lower, the crack widths decrease. Due to the residual deformation of the dam (Fig. 22), the cracks did not close after the earthquake. The distribution of residual crack of the face slab after the earthquake is depicted in Fig. 23 and the crack widths at $0.73H$ and at $0.84H$ are 4.0 mm and 0.8 mm, respectively.

Two cracks can be observed on the face slab and their maximum widths are reached at different times (Fig. 19). The evolution of the total crack widths (sum of crack widths at the slab) in the slab during the earthquake is shown in Fig. 24. It is observed that the maximum total

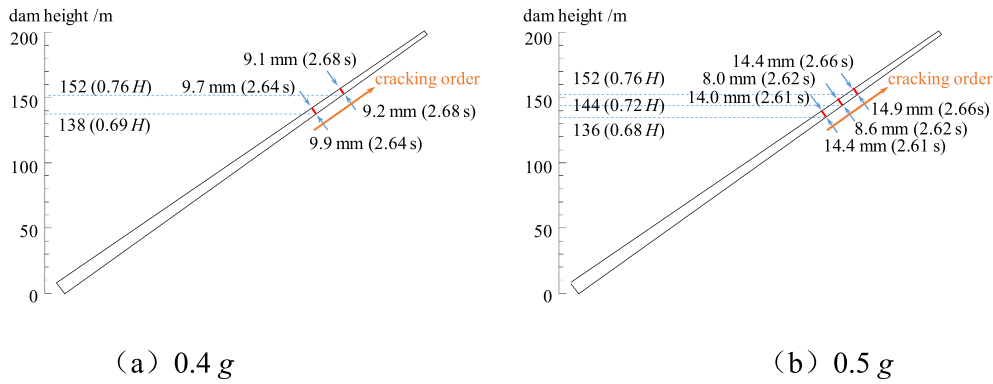


Fig. 28. Crack location, max crack width and initial cracking moment for reinforced concrete face slab during earthquakes of different PGAs.

crack width during the earthquake is 22.3 mm at 11.36 s and residual maximum crack width after the earthquake is 5.9 mm.

The method developed in this paper can simulate the evolution of cracks on the concrete face slab as well as the decrease of the crack width after the earthquake. In addition, the cracking area and the crack severity can be accurately located and directly quantified.

5.2. Influence of the steel reinforcement

In the CFRD, the anti-seepage slab is usually made of reinforced concrete. This section studies the influence of the rebar on the damage of the face slab during an earthquake. The bidirectional reinforcement ratio is 1.4%. The rebar is simulated using an ideal elasto-plastic model with elastic modulus $E = 200$ GPa and yield strength $f_y = 400$ MPa [5].

The crack location, initial cracking moment, and maximum crack width of the reinforced concrete face slab during the earthquake are provided in Fig. 25. The crack occurs at $0.71H$ of the face slab, with a maximum crack width of 5.6 mm. The crack propagates through the thickness of the face slab. The crack width and time of occurrence are the same on both sides of the face slab.

The time history of the displacement of the cracking elements, the axial stress of steel (include static response), the concrete stress (include static response) along the slope and the stiffness degradation coefficient of concrete at the upstream side of the face slab are shown in Fig. 26. The concrete is damaged at 4.24s, which is later than that of the concrete face slab (2.70s). The reason for the delay is that the rebar sustains a part of the tension force. The increase of ground motion intensity and accumulation of residual deformation of the dam aggravates the concrete damage, and causes the stiffness of the concrete to degrade and the tension of rebar to increase. The concrete completely fails at 11.36s and loses the resistance to tension. Meanwhile, although the rebar yielded, it

can still bear a portion of the tension, thus limiting the cracking at the slab. Therefore, the maximum crack width of the reinforced concrete face slab is much smaller than that of the concrete face slab. The residual crack pattern after the earthquake is shown in Fig. 27 and the maximum crack width is 1.0 mm.

Compared to the concrete face slab, the maximum and residual total crack width on the reinforced concrete face slab is reduced by 75.6% and 83.1%, respectively, the cracking elevation is lower and the initial cracking moment is delayed. However, the time to reach the maximum crack width in both cases are almost the same.

5.3. Influence of ground motion

Fig. 28 shows the crack location, maximum crack width and initial cracking moment of the reinforced concrete face slab for the PGA of 0.4 g and 0.5 g. The residual crack pattern is depicted in Fig. 29. In comparing Figs. 28 and 23, the damaged areas can be observed to be similar for different PGAs. However, the cracking elevation is lower with the increase of PGA. Meanwhile, when the failure pattern consists of multiple cracks, the order of cracking is from lower to higher elevation. The influence of PGA on the crack width of reinforced concrete face slab is listed in Table 6. As the PGA increases, both the individual crack width and total crack width increase. Comparing items (3) and (5) in Table 6, it can be observed that with the increase of PGA, the crack width increases at a more rapid rate; thus indicating an increasing influence of PGA on the crack width.

The time history of the total crack width for the upstream face slab during the earthquake is shown in Fig. 30. The greater the PGA, the earlier the face slab cracks. The characteristic of the crack evolution and moment in which the maximum total crack width appeared are similar with the different PGAs.

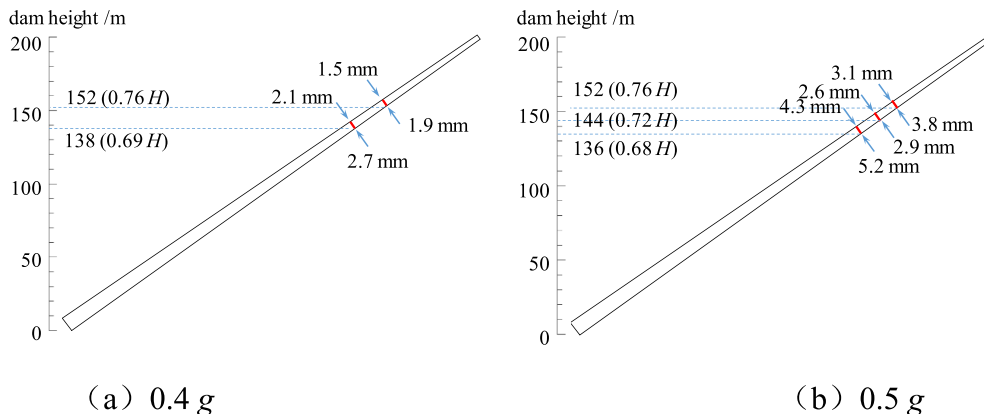


Fig. 29. Distribution of cracks on the reinforced concrete face slab after the earthquakes of different PGAs.

Table 6

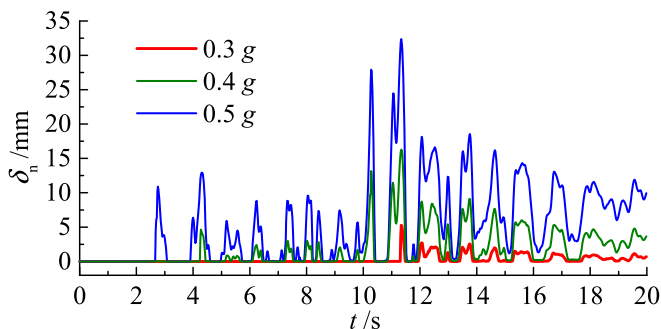
Effect of peak ground acceleration on face slab cracking.

Peak ground acceleration/g	0.3	0.4	0.5	
	(1)	(2)	(3) = (2) – (1)	(4) = (4) – (2)
Maximum individual crack width/mm	5.6	9.9	4.3	14.9
Maximum total crack width/mm	5.6	16.6	11.0	33.5
Maximum individual residual crack width/mm	1.0	2.7	1.7	5.2
Maximum total residual crack width/mm	1.0	4.6	3.6	11.9

6. Conclusion

In this paper, the CZM combined with generalized plastic models of rockfill and interface is extended to investigate the seismic cracking evaluation for the slabs in CFRDs. An explicit SBFEM-FEM is developed to enable cross-scale analysis. The method can consider the strain softening of rockfill and concrete after being damaged and avoids the occurrence of negative stiffness and the convergence problems that are present in implicit analysis. The elasto-plastic seismic cracking evolution of face slab is investigated in detail with consideration to the steel reinforcement and ground motion intensity.

- 1) The dynamic stress of the face slab is mainly generated by the friction from the cushions. The damping ratio of the face slab has very limited influence on the dynamic response of the CFRD. Therefore, it is feasible to decrease the damping ratio of the face slab to improve the computation efficiency in the explicit dynamic analysis of the CFRD.
- 2) Compared to the commonly used elastic model for face slab analysis, the proposed method offers an improvement on failure analysis in the area of CFRD numerical simulation. The computed stress in the slab does not exceed the tensile strength of concrete. The stiffness degradation and strain softening are considered. The computed failure mode of the slab agrees well with the material characteristics of concrete.
- 3) Penetrating cracks are observed on the slab, and the crack widths and initial cracking moments at both sides of the slab are almost the same. The crack reaches the maximum width during the earthquake, and a residual width is retained after the earthquake.
- 4) Compared to the concrete face slab, the maximum and residual total crack width on the reinforced concrete face slab is reduced by 75.6% and 83.1%, respectively. Furthermore, the cracking elevation is lower, and the initial cracking moment is delayed. However, the time to reach the maximum crack width in both cases are almost the same.
- 5) The damaged areas are similar for different PGAs. As the PGA increases, the crack appears earlier. Furthermore, both the individual crack width and the total crack width increase, and the influence of

**Fig. 30.** Total crack width over time for different peak ground accelerations.

PGA on the crack width increases. The characteristics of the total crack width evolution is similar. When the failure pattern consists of multiple cracks, the cracking occurs from the order of low to high elevation.

- 6) The presented method can describe the crack evolution during the earthquake in detail, accurately locate the weak areas of the face slab, quantitatively evaluate the degree of damage and estimate the anti-seismic capacity and reinforcement measures of the CFRD. In addition, the method can provide guidance for risk assessment (e.g. seepage induced damage, dam collapse) of dams.
- 7) The proposed method can be utilized for the analysis of other concrete anti-seepage structures (e.g. connection wall, anti-seepage wall), as well as the analysis of concrete cracking involving soil-concrete interaction.
- 8) The method can be straightforwardly extended for three-dimensional analysis and avoid the issue of scalar damage factors, which can cause the loss of stiffness and bearing capacity in the other two directions when only one direction is damaged. Future work will aim towards three-dimensional failure analyses of CFRDs to investigate damage localization, damage mechanisms, influencing factors of face slab safety, as well as anti-seismic measures.

Declaration of competing interest

The authors declare that they have no known competing financial interests or personal relationships that could have appeared to influence the work reported in this paper.

CRediT authorship contribution statement

Yongqian Qu: Software, Methodology, Formal analysis, Investigation, Data curation, Writing - original draft, Visualization. **Degao Zou:** Conceptualization, Software, Methodology, Validation, Writing - review & editing, Project administration, Funding acquisition. **Xianjing Kong:** Conceptualization, Resources, Supervision, Validation. **Xiang Yu:** Software. **Kai Chen:** Writing - review & editing.

Acknowledgements

The research work described in this paper was supported by the National Natural Science Foundation of China (Grant Nos. U1965206, 51779034) and the Fundamental Research Funds for the Central Universities (Grant No. DUT19ZD216). The writers would like to greatly acknowledge all the financial support and express their sincerest gratitude.

References

- [1] Zarfi C, Lumsdon AE, Berlekamp J, et al. A global boom in hydropower dam construction. *Aquat Sci* 2015;77(1):161–70.
- [2] Kim Y, Kim B. Prediction of relative crest settlement of concrete-faced rockfill dams analyzed using an artificial neural network model. *Comput Geotech* 2008;35(3): 313–22.
- [3] Qu Y, et al. Seismic damage performance of the steel fiber reinforced face slab in the concrete-faced rockfill dam. *Soil Dynam Earthq Eng* 2019;119:320–30.
- [4] Kong Xian-Jing, Zhou Yang, De-Gao Zou, et al. Numerical analysis of dislocations of the face slabs of the Zipingpu concrete faced rockfill dam during the Wenchuan earthquake. *Earthq Eng Eng Vib* 2011;10(4):581–9.
- [5] Zou Degao, Zhou Yang, Ling Hoe I, et al. Dislocation of face-slabs of Zipingpu concrete face rockfill dam during Wenchuan earthquake. *J Earthq Tsunami* 2012;6 (2):1–17.
- [6] Arrau L, Ibarra I, Noguera G. Performance of Cogoti dam under seismic loading// Concrete face rockfill dams—design, construction, and performance. ASCE; 1985. p. 1–14.
- [7] Saberi M, Annan CD, Konrad JM. Seismic response analysis of face slabs in concrete face rockfill dams[J]. *J Earthq Eng* 2019:1–29.
- [8] Xu B, et al. Dynamic damage evaluation on the slabs of the concrete faced rockfill dam with the plastic-damage model. *Comput Geotech* 2015;65:258–65.
- [9] Dakoulas P. Longitudinal vibrations of tall concrete faced rockfill dams in narrow canyons. *Soil Dynam Earthq Eng* 2012;41:44–58.

- [10] Lee J, Fenves GL. Plastic-damage model for cyclic loading of concrete structures. *J Eng Mech* 1998;124(8):892–900.
- [11] Arici Y. Investigation of the cracking of CFRD face plates. *Comput Geotech* 2011;38(7):905–16.
- [12] Cen W, et al. Numerical simulation of seismic damage and cracking of concrete slabs of high concrete face rockfill dams. *Water Sci Eng* 2016;9(3):205–11.
- [13] Barenblatt GI. The mathematical theory of equilibrium cracks in brittle fracture. *Advances in applied mechanics*, vol. 7. Elsevier; 1962. p. 55–129.
- [14] Dugdale DS. Yielding of steel sheets containing slits. *J Mech Phys Solid* 1960;8(2):100–4.
- [15] Hillerborg A, Modeer M, Peterson E. Analysis of crack formation and crack growth in concrete by means of fracture mechanics and finite elements. *Cement Concr Res* 1976;6:773–82.
- [16] Dai Q, Ng K. 2D cohesive zone modeling of crack development in cementitious digital samples with microstructure characterization. *Construct Build Mater* 2014;54:584–95.
- [17] Pan J, Zhang C, Xu Y, et al. A comparative study of the different procedures for seismic cracking analysis of concrete dams. *Soil Dynam Earthq Eng* 2011;31(11):1594–606.
- [18] Kim H, Wagoner MP, Buttlar WG. Simulation of fracture behavior in asphalt concrete using a heterogeneous cohesive zone discrete element model. *J Mater Civ Eng* 2008;20(8):552–63.
- [19] Su X, Yang Z, Liu G. Finite element modelling of complex 3D static and dynamic crack propagation by embedding cohesive elements in Abaqus. *Acta Mech Solida Sin* 2010;23(3):271–82.
- [20] Yilmaz O, Molinari JF. A mesoscale fracture model for concrete. *Cement Concr Res* 2017;97:84–94.
- [21] Trawinski W, Teichman J, Bobinski J. A three-dimensional meso-scale modelling of concrete fracture, based on cohesive elements and X-ray μ CT images. *Eng Fract Mech* 2018;189:27–50.
- [22] Kim YR, De Freitas FAC, Jung JS, et al. Characterization of bitumen fracture using tensile tests incorporated with viscoelastic cohesive zone model. *Construct Build Mater* 2015;88:1–9.
- [23] Kim SM, Al-Rub RKA. Meso-scale computational modeling of the plastic-damage response of cementitious composites. *Cement Concr Res* 2011;41(3):339–58.
- [24] Zhong H, Li H, Ooi ET, et al. Hydraulic fracture at the dam-foundation interface using the scaled boundary finite element method coupled with the cohesive crack model. *Eng Anal Bound Elem* 2018;88:41–53.
- [25] Guo SS, Chen HQ, Li DY, et al. Study of element-size effect on dynamic plastic-damage analysis of concrete. *J Hydroelectr Eng* 2011;30(6):52–6.
- [26] Qu Y, Zou D, Kong X, et al. A novel interface element with asymmetric nodes and its application on concrete-faced rockfill dam. *Comput Geotech* 2017;85:103–16.
- [27] Chen K, Zou D, Kong X, et al. Global concurrent cross-scale nonlinear analysis approach of complex CFRD systems considering dynamic impervious panel-rockfill material-foundation interactions. *Soil Dynam Earthq Eng* 2018;114:51–68.
- [28] Zhou M, Zhang B, Peng C, et al. Three-dimensional numerical analysis of concrete-faced rockfill dam using dual-mortar finite element method with mixed tangential contact constraints. *Int J Numer Anal Methods GeoMech* 2016;40(15):2100–22.
- [29] Qu YQ, Zou DG, Kong XJ, et al. A flexible various-scale approach for soil-structure interaction and its application in seismic damage analysis of the underground structure of nuclear power plants. *Sci China Technol Sci* 2018;61(7):1092–106.
- [30] Chen K, Zou DG, Kong XJ, et al. A novel nonlinear solution for the polygon scaled boundary finite element method and its application to geotechnical structures. *Comput Geotech* 2017;82:201–10.
- [31] Chen K, Zou DG, Kong XJ. A nonlinear approach for the three-dimensional polyhedron scaled boundary finite element method and its verification using Koyna gravity dam. *Soil Dynam Earthq Eng* 2017;96:1–12.
- [32] Chen K, Zou DG, Kong XJ, et al. An efficient nonlinear octree SBFEM and its application to complicated geotechnical structures. *Comput Geotech* 2018;96:226–45.
- [33] Chen K, Zou DG, Kong XJ, et al. Elasto-plastic fine-scale damage failure analysis of metro structures based on coupled SBFEM-FEM. *Comput Geotech* 2019;108:280–94.
- [34] Wolf JP, Song CM. Finite-element modelling of unbounded media. Chichester: Wiley; 1996.
- [35] Wolf JP, Schanz M. The scaled boundary finite-element method. Chichester, U.K: Wiley; 2004.
- [36] Man H, Song C, Gao W, et al. A unified 3D-based technique for plate bending analysis using scaled boundary finite element method. *Int J Numer Methods Eng* 2012;91(5):491–515.
- [37] Liu Y, Saputra AA, Wang J, et al. Automatic polyhedral mesh generation and scaled boundary finite element analysis of STL models. *Comput Methods Appl Mech Eng* 2017;313:106–32.
- [38] Saputra A, Talebi H, Tran D, et al. Automatic image-based stress analysis by the scaled boundary finite element method. *Int J Numer Methods Eng* 2017;109(5):697–738.
- [39] Liu J, Zhang P, Lin G, et al. Solutions for the magneto-electro-elastic plate using the scaled boundary finite element method. *Eng Anal Bound Elem* 2016;68:103–14.
- [40] Liu Jun, Gao Lin. A scaled boundary finite element method applied to electrostatic problems. *Eng Anal Bound Elem* 2012;36(12):1721–32.
- [41] Shi M, Zhong H, Ooi ET, et al. Modelling of crack propagation of gravity dams by scaled boundary polygons and cohesive crack model. *Int J Fract* 2013;183(1):29–48.
- [42] Pastor M, Zienkiewicz OC, Leung KH. Simple model for transient soil loading in earthquake analysis. II. Non-associative models for sands. *Int J Numer Anal Methods GeoMech* 1985;9:477–98. <https://doi.org/10.1002/nag.1610090506>.
- [43] Pastor M, Zienkiewicz OC. A generalized plasticity, hierarchical model for sand under monotonic and cyclic loading. *Proceedings of the 2nd International Symposium on Numerical Models in Geomechanics*, Ghent. 1986. p. 131–49.
- [44] Xu B, Zou D, Liu H. Three-dimensional simulation of the construction process of the Zipingpu concrete face rockfill dam based on a generalized plasticity model. *Comput Geotech* 2012;43:143–54. <https://doi.org/10.1016/j.compgeo.2012.03.002>.
- [45] Xu B, Zhou Y, Zou D. Numerical simulation on slabs dislocation of Zipingpu concrete faced rockfill dam during the Wenchuan earthquake based on a generalized plasticity model. *Sci World J* 2014;2014:572407.
- [46] Zou D, Xu B, Kong X, Liu H, Zhou Y. Numerical simulation of the seismic response of the Zipingpu concrete face rockfill dam during the Wenchuan earthquake based on a generalized plasticity model. *Comput Geotech* 2013;49:111–22. <https://doi.org/10.1016/j.compgeo.2012.10.010>.
- [47] Liu H, Ling HI. Constitutive description of interface behavior including cyclic loading and particle breakage within the framework of critical state Soil mechanics. *Int J Numer Anal Methods GeoMech* 2008;32:1495–514. <https://doi.org/10.1002/nag.682>.
- [48] Liu H, Song E, Ling HI. Constitutive modeling of soil-structure interface through the concept of critical state Soil mechanics. *Mech Res Commun* 2006;33:515–31. <https://doi.org/10.1016/j.mechrescom.2006.01.002>.
- [49] Liu J, Zou D, Kong X. A three-dimensional state-dependent model of soil-structure interface for monotonic and cyclic loadings. *Comput Geotech* 2014;61:166–77. <https://doi.org/10.1016/j.compgeo.2014.05.012>.
- [50] Du J, Yon JH, Hawkins NM, Arakawa K, Kobayashi AS. Fracture process zone for concrete for dynamic loading. *ACI Mater J* 1992;89(3):252–8.
- [51] Chen K, Zou D, Kong X, et al. A novel nonlinear solution for the polygon scaled boundary finite element method and its application to geotechnical structures. *Comput Geotech* 2017;82:201–10.
- [52] Zou D, Teng X, Chen K, et al. An extended polygon scaled boundary finite element method for the nonlinear dynamic analysis of saturated soil. *Eng Anal Bound Elem* 2018;91:150–61.
- [53] Ooi ET, Man H, Natarajan S, et al. Adaptation of quadtree meshes in the scaled boundary finite element method for crack propagation modelling. *Eng Fract Mech* 2015;144:101–17.
- [54] Qu Y, Zou D, Kong X, et al. A novel interface element with asymmetric nodes and its application on concrete-faced rockfill dam. *Comput Geotech* 2017;85:103–16.
- [55] Westergaard HM. Water pressures on dams during earthquakes. *Translator* 1933;98:418–33.
- [56] Lu Y, Liu J. A direct method for analysis of dynamic soil-structure interaction. *China Civ Eng J* 1998;3. 008.
- [57] Xu B, Zhou Y, Zhou C, et al. Dynamic responses of concrete-faced rockfill dam due to different seismic motion input methods. *Int J Distributed Sens Netw* 2018;14(10). 1550147718804687.
- [58] Idriss IM. Quad-4: a computer program for evaluating the seismic response of soil structures by variable damping finite element procedures[M]. University of California; 1973.
- [59] Zou D, Xu B, Kong X. Study of influence of different methods for calculating Rayleigh damping coefficient on high earth-rock dam seismic response. *Rock Soil Mech* 2011;32:797–803. 03.
- [60] Hudson M, Idriss IM, Mohsen Beiken. User manual for Quad4m: a computer program to evaluate the seismic response of soil structures using finite element procedures and incorporating a compliant base. California: University of California; 1994.
- [61] Zhang Y, Kong X, Zou D, et al. Tensile stress responses of CFRD face slabs during earthquake excitation and mitigation measures. *Int J GeoMech* 2017;17(12):04017120.